Biophysical Journal, Volume *113*

Supplemental Information

Is Aggregate-Dependent Yeast Aging Fortuitous?

A Model of Damage Segregation and Aggregate Dynamics

Martín Andrade-Restrepo

Supplemental Information and Supporting Figures

S1 Numerical methods and dependence on numerical parameters

S1.1 Short-term single division cycle

In the simulations of the short-term, single-division-cycle aggregate dynamics of our passive-only model we first introduce the organelles inside the mother cell as spheres centered at a random position. The centers of organelles are computed using a uniform distribution inside a sphere of radius $r_m - r_o$, where r_o is the radius of the organelle and r_m the radius of the mother cell. Organelles are not allowed to overlap with other organelles and therefore their centers must lie at a distance larger that the addition of their radii. Next, we set an initial number of aggregates N, represented by spheres with radius r_a^i, with centers computed from a uniform distribution inside a sphere of radius $r_m - r_a^i$, again with the restriction that they cannot overlap or lie inside the organelles.

Aggregates are generated randomly inside the mother and bud compartments at times taken from exponential distributions with rates $\frac{1}{\tau_m}$ and $\frac{1}{\tau_b}$ respectively. Each time this occurs, the position of the aggregate is generated randomly from a uniform distribution in each compartment –in the case of the bud, the centers are computed using a uniform distribution inside a sphere with radius $r_b(t) - r_a^i$ and which is centered at $(x_b(t), y_b(t), z_b(t))$ which denotes the bud's focus.

Aggregates undergo diffusion, with a time step of length δt (see Fig. S1) and diffusion coefficient $D(r_i(t)) = \frac{\beta}{r_i(t)^\gamma}$, taken from (1). As measured in (1), the values for β and γ are different from $\beta = \frac{k_B T_e}{6\pi\mu}$ and $\gamma = 1$, which correspond to the traditional Stokes-Einstein equation (T_e being the absolute temperature). Additionally we increase the radii of all aggregates following $r_i(t) = (\frac{3}{4\pi} C_c \delta t + r_i(t - \delta t)^3)^{\frac{1}{3}}$ where $C_c = \frac{4\pi (r_a^i)^3}{3\tau_m}$ or $C_c = \frac{4\pi (r_a^i)^3}{3\tau_d}$ depending on the compartment. These growth rates are chosen so that, in absence of fusion and cross-compartment crossings, aggregates will have a radius r_a^i after a time τ_c.

Upon contact of aggregates i and j (when the distance between aggregate centers is smaller that the sum of their radii), binding happens with a probability p_b. If this is the case, a new aggregate of radius $(r_i(t)^3 + r_j(t)^3)^{\frac{1}{3}}$ is generated at the intermediate position. In the case of collision against the cell walls (mother or bud) or against an organelle, the position of the aggregate is recalculated assuming a completely elastic collision against the boundary. We also considered the case where a fraction e_l of the energy was lost by setting the distance after the impact to be $l_2^* = l_2(1 - e_l)$, l_2 being the distance after a completely elastic collision, but the results were not substantially different, with the exception of a small increase in the amount of cross-compartment crossings (see Fig. S2).

The process above is continued until a time T is reached, corresponding to the time at which the neck connecting both cells closes. Meanwhile, the radius of the daughter cell –with initial value $r_d(0) = \frac{l_n}{2} + \varepsilon$– grows progressively until it reaches its final value $r_d(T)$ at the end of the process. The value of the parameter $r_d(0)$ was chosen so that the center of the daughter cell was at a distance larger than r_m from the center of the mother cell. In order to keep the length of the neck constant, the position of the center of the daughter cell is varied.

S1.2 Long-term yeast life cycle

The long-term simulations of the passive-only model have the following structure. Initially, cells are born with zero aggregates. Before the first division and in-between divisions, similarly as in (1, 2), fusion of pre-existing aggregates i and j of radii $r_i(0)$, $r_j(0)$ may occur with rate:

$$K(i,j) = p_b \frac{4\pi}{V} (D(r_i(0)) + D(r_j(0)))(r_i(0) + r_j(0)), \tag{S1}$$

where V is the volume of the domain in which they are allowed to diffuse (approximately the volume of the mother minus the volumes of organelles). Here, $r_i(0)$ is not necessarily equal to r_a^i but to the radius of aggregate i at the end of the last division. Additionally, at the end of this period of duration T_s, pre-existing aggregates' radii are increased to a value $r_i(t+T_s) = (\frac{3}{4\pi}C_m T_s + r_i(0)^3)^{\frac{1}{3}}$ and a random number of aggregates taken from a Poisson distribution with mean $\frac{T_s}{\tau_m}$ are generated with initial radii r_a^i. During this period, we generate the event times with a constant rate. The precision of this approximation becomes considerable when the rate of growth is small, as is the case for WT unperturbed cells. After the period between two consecutive division cycles, we run the single-division dynamics described in Section S1.1.

S1.3 Dependence on δt

In Fig. S1 we show the dependence of the short-term simulation results when varying the parameter δt. At short and intermediate timescales the MSD is similar for all values of the time-step size. At longer timescales, for $\delta t = 1$ sec., there appears to be an overestimation of aggregate motion as shown in Fig. S1A. Concerning aggregate numbers, for larger values of δt, fusion is underestimated as a consequence of overlooked collisions. Nevertheless, after sufficient time, for values smaller than $\delta t = 0.5$ sec. all trajectories converge to similar values after a sufficiently long time. This underestimation of aggregate collisions impacts the aggregate volume in the mother cell as well (Fig. S1E). Indeed, for having constant rates of growth for aggregates of all sizes, two aggregates increase in volume at twice the rate of one larger aggregate. We claim that this does not impact strongly the results shown above since aggregate numbers are always low (close to 1 or 2) given the frequency of fusion and that for smaller growth rates the error becomes negligible. In the case where aggregate volume becomes significantly overestimated, we also provide a variant of the model and the mathematical approximation where aggregate growth increases with the surface area of the aggregate (Section S8). In this case –although in general, rates must be smaller (due to the exponential growth of volume)– all the conclusions remain unvaried.

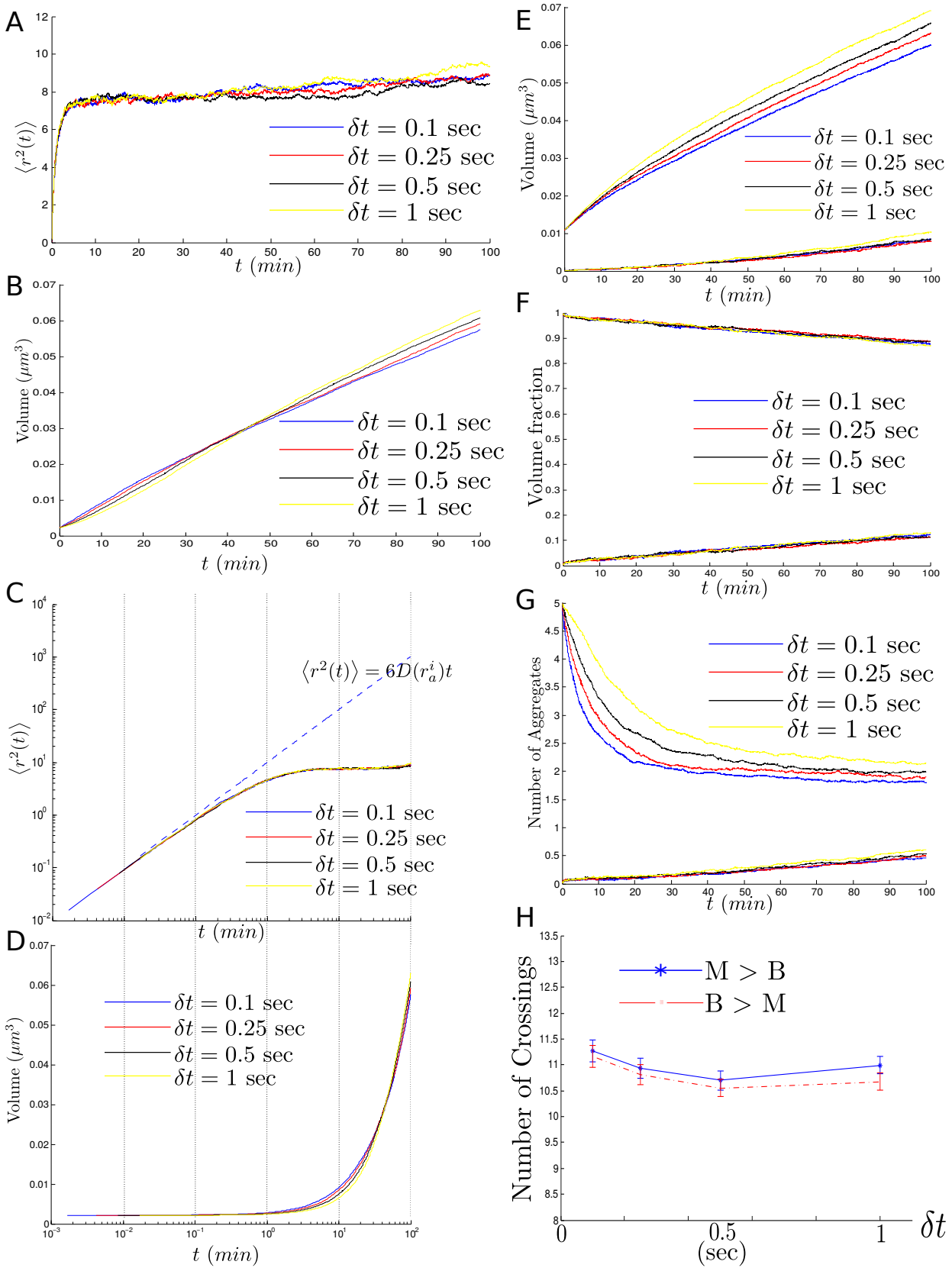

Figure S1: Dependence on δt. A-D. MSD of one aggregate throughout the simulation of the single-division component of the model (top) and volume of the same aggregate for which the MSD was computed (bottom) for different values of δt. F-G. Log-log plot of Fig. S1A-S1B. Dashed lines correspond to the MSD of an aggregate of radius r_a^i. E-G. Total aggregate volume, fraction of the total aggregate volume and number of aggregates inside the mother and the daughter cell for different values of δt. H. Total number of cross-compartment events from mother to bud ($M > B$) and from bud to mother ($B > M$) as a function of δt. In all figures, $N = 5$, $\tau_m = 12$ min., $\tau_d = 120$ min. All other parameters were set to the values in Table S1. Results averaged over 1024 realizations.

S2 Mathematical Analysis

From (3) we know that the first order approximation of the mean-first-passage-time (MFPT) of a particle undergoing diffusion in a domain of volume V follows $\mathbb{E}(\tau) = \frac{V}{2lD}(1 + o(1)) \simeq \frac{V}{2lD}$, where l denotes the diameter of the disc through which particles can escape and D denotes the diffusion coefficient. Due to the possibility of recrossings at the open window where the probability of movement in both directions is equal, the rate of exit from the domain is $\kappa = \frac{1}{2\mathbb{E}(\tau)} \simeq \frac{lD}{V}$ (4). If besides undergoing diffusion, aggregates also appear and fuse on collision, we can model inner-cell aggregate dynamics using a system of coupled differential equations. Let $V_m^a(t)$, $V_d^a(t)$ be the total aggregate volume (detected) at mother and daughter cells at a time t. In addition, let $N_m(t)$, $N_d(t)$ be the total number of aggregates in each compartment. We abuse notation by denoting $\mathbb{E}(N_m(t))$, $\mathbb{E}(N_d(t))$ by $N_m(t)$ and $N_d(t)$, and $\mathbb{E}(V_m^a(t))$, $\mathbb{E}(V_d^a(t))$ by $V_m^a(t)$, $V_d^a(t)$. Lets define $\langle V(t)\rangle_m = V_m^a(t)/N_m(t)$, $\langle V(t)\rangle_d = V_d^a(t)/N_d(t)$ as the average volume of an aggregate in the mother and the daughter cell respectively at a time t. We assume that all aggregates in the mother have radius $r_m(t) = (\frac{3\langle V(t)\rangle_m}{4\pi})^{\frac{1}{3}}$ and diffusion coefficient $D(r_m(t)) = \frac{\beta}{r_m(t)^\gamma}$. Likewise, aggregates inside the daughter all have radius equal to $r_d(t) = (\frac{3\langle V(t)\rangle_d}{4\pi})^{\frac{1}{3}}$ and diffusion coefficient $D(r_d(t)) = \frac{\beta}{r_d(t)^\gamma}$. If $V_1 = V_m - V_v - V_n$ denotes the volume of the mother cell inside which aggregates undergo diffusion and $V_2(t)$ denotes the volume of the daughter at a time t then we can model the dynamics of $N_m(t)$, $N_d(t)$, $V_m^a(t)$, $V_d^a(t)$ as:

$$\begin{cases} \frac{dN_m(t)}{dt} = \frac{1}{\tau_m} - p_b N_m(t)\max(N_m(t)-1,0)\frac{16\pi r_m(t)D(r_m(t))}{V_1} - \kappa_m(t)N_m(t) + \kappa_d(t)N_d(t) \\ \frac{dN_d(t)}{dt} = \frac{1}{\tau_d} - p_b N_d(t)\max(N_d(t)-1,0)\frac{16\pi r_d(t)D(r_d(t))}{V_2(t)} - \kappa_d(t)N_d(t) + \kappa_m(t)N_m(t) \\ \frac{dV_m^a(t)}{dt} = C_m N_m(t) - \kappa_m(t)N_m(t)\langle V(t)\rangle_m + \kappa_d(t)N_d(t)\langle V(t)\rangle_d + \frac{1}{\tau_m}V_a^i \\ \frac{dV_d^a(t)}{dt} = C_d N_d(t) - \kappa_d(t)N_d(t)\langle V(t)\rangle_d + \kappa_m(t)N_m(t)\langle V(t)\rangle_m + \frac{1}{\tau_d}V_a^i \end{cases} \tag{S2}$$

Where $\kappa_m = \frac{(l_n - 2r_m(t))^+ D(r_m(t))}{V_1}$ is the escape rate from the mother, $\kappa_d(t) = \frac{(l_n - 2r_d(t))^+ D(r_d(t))}{V_2(t)}$ the escape rate of the daughter and V_a^i the volume of an aggregate with radius r_a^i. The second term on the right of the equality in the first two equations corresponds to rate of fusion in each one of the two domains, which was introduced in Eq. S1. Here, the constant 16π is a consequence of the assumption that all aggregates in each of the compartments have equal radius and equal diffusion coefficient.

S3 Parameter Values of the Model

The parameter values used in the simulations of the model are shown in Table S1.

Parameter	Interpretation	Value	Source	Additional comments
r_m	Radius of mother cell	2.5 μm	T.N.	
$r_d(T)$	Final radius of daughter cell	1.9 μm	T.N.	
r_v	Radius of vacuole	1.1 μm	T.N.	
r_n	Radius of nucleus	0.9 μm	T.N.	
l_n	Length of neck	1.35 μm	T.N.	
$r_{d_0} = r_d(0)$	Initial radius of daughter cell	$\frac{l_n}{2} + 0.025$ μm	-	The radius of the daughter must be larger than half the size of the neck.
T	Duration of cell division	100 min	T.N.	
r_a^i	Detection threshold (initial radius of aggregate)	0.08 μm	(1)	Estimated after a temperature shift from 30^{o}C to 38^{o}C using time-lapse microscopy to observe the fluorescence intensity of foci. Since the initial volume is $v_a^i = (0.01)(0.6\ \mu m)^3$, then $r_a^i = 0.08\ \mu m$.
T_s	Time between two cell division cycles	45 min	(5, 6)	Two successive cell divisions occur with a difference of 145 mins. Since we set $T = 100$ min we leave $T_s = 45$ min. This is consistent with Fig. 3A in (6) for WT unperturbed cells.
τ_m	Average time of appearance of aggregates in mother cell	12 min, 25 min, 50 min, 100 min, 200 min, 400 min, 800 min	(7)	Around 30% of cells form an aggregate after 1-2 divisions and thus $\tau_m \simeq 800\ min$ in WT cells and $\tau_m \ll 800\ min$ after stress.
τ_d	Average time of appearance of aggregates in daughter cell	$10 \times \tau_m$	-	
β	Constant in functional relation between diffusion coefficient and radius of aggregate	1.4×10^{-4}	(1)	Estimated after a temperature shift from 30^{o}C to 38^{o}C using time-lapse microscopy and image analysis.
γ	Power of radius of aggregate in functional description of diffusion coefficient	2.1	(1)	Same as with β.
$D(r(t))$	Diffusion coefficient for an agg. with radius $r(t)$	$D(r(t)) = \beta / r(t)^\gamma$	(1)	Same as with β and γ
N_{death}	Number of cell divisions before death	28 divisions	(7, 8)	
p_b	Probability of fusion in case of collision	0.9	(2)	The reference value used was estimated in fission yeast after wide-field fluorescence microscopy.
e_l	Proportion of energy lost in case of collision against boundary or organelles	0	-	
p_s	Probability of movement only in direction of mother cell's pole (every time step)	0.05	-	
p_c	Probability of remaining confined to organellar surfaces for every passing minute	1	-	
d_c	Maximum distance between center of the aggregate and surface of organelle for possible confinement to organellar surface	0.3 μm	-	
p_a	Probability of attachment to cell membrane in case of collision	0.5	-	
p_w	Probability of remaining attached to cell membrane after adhesion to organellar surfaces for every passing minute	0.9	-	

Table S1: Model parameters, values and sources. T.N refers to a personal communication with T. Nyström, Department of Cell and Molecular Biology–Microbiology, Göteborg University, Göteborg, Sweden. March 2012.

S4 Dependence on e_l

We show in Fig. S2 the results of the simulations of the short-term component of our model when varying the fraction of energy lost after collision against organelles or the cell's boundary. All statistics appear to be independent of the parameter e_l, except the number of crossings which has a subtle increase for higher values of this parameter. This is likely to be a consequence of aggregates remaining close to the neck once they collide to the cell walls in its vicinity.

S5 Dependence on the diffusion coefficient

We complement the observations concerning the dependence of the model on the diffusion rate with the results shown in Fig. S3. For higher diffusion rates, the number of aggregates in the mother and the daughter is low as a consequence of increased fusion.
Concerning aggregate volumes, at high diffusion rates, the volume in the mother decreases as its retention capacity is diminished. This produces an increase in aggregate volumes inside the daughter. At low diffusion rates, aggregates remain inside the mother and do not cross to the bud and thus aggregate volumes are higher in the mother compartment. Nevertheless, the fraction of volume in each compartment does not change substantially. This is a consequence of the high aggregation rates and of the constant growth in volume of existing aggregates.

S6 Aggregate kinetics under no cross-compartment movement and under no fusion

In Fig. 3A, when comparing the slopes of both curves after 40 min., we observe that the growth rate in the mother cell is approximately 6 times higher than the growth rate in the daughter cell. Under small or non-existent cross-compartment movement, given that the rates differ in a tenfold, the ratio would be expected to be over 10 instead. Thus, cross-compartment transport reduces substantially the difference between the appearance rates, the growth rates and the initial number of aggregates between the two cells.

We show in Fig. S4 the aggregate dynamics of the single-division component when assuming no compartmental crossings (i.e a closed neck) in our model. Under this assumption, the effect of bud-specific dilution, represented by the difference in the aggregate generation and growth rates, on the asymmetrical distribution of damage is substantially stronger, as can be confirmed in Fig. S4C. Moreover, aggregate numbers would be overestimated in the daughter cell (Fig. S4A) due to the lack of escape, and aggregate volume overestimated and underestimated in the mother and daughter cells respectively (Fig. S4B).

With respect to a model without fusion or appearance of new aggregates as in (14, 15), under the diffusion rates measured in (1), asymmetrical partitioning of volume would be substantially reduced to 68%-32% (measured with equations (S2)). This yields a probability of approximately 0.32 for each aggregate to be inherited by the bud, which is not in agreement with experimental quantifications (16).

Hence, both bud-specific dilution and cross-compartment movement have an important role in the compartmental distribution of aggregate volumes, although their strength may vary depending on the experimental conditions (the rate $1/\tau_m$). We then suggest that both should be considered when modeling the asymmetrical distribution of aggregates in budding yeast.

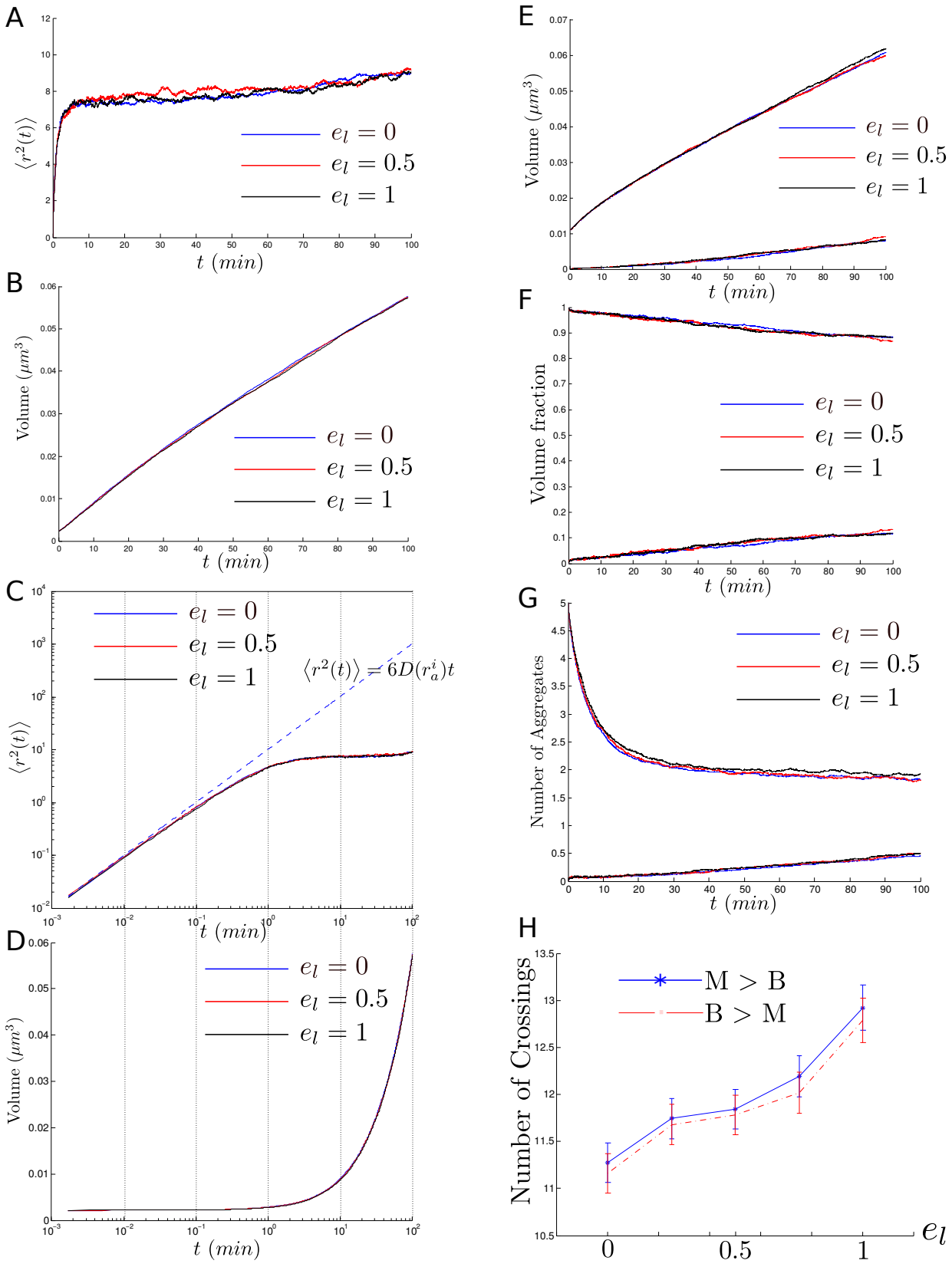

Figure S2: Dependence on e_l. A-D. MSD of one aggregate throughout the single-division cycle simulation of the model and volume of the same aggregate for which the MSD was computed (bottom) for different values of e_l. F-G. Log-log plot of Fig. S2A-S2B. Dashed lines correspond to the MSD of an aggregate of radius r_a^i. E-G. Total aggregate volume, fraction of the total aggregate volume and number of aggregates inside the mother and the daughter cell for different values of e_l. H. Total number of cross-compartment events from mother to bud ($M > B$) and from bud to mother ($B > M$) as a function of e_l. In all figures, $N = 5$, $\delta t = 0.1$ sec., $\tau_m = 12$ min., $\tau_d = 120$ min. All other parameters were set to the values in Table S1. Results averaged over 1024 realizations.

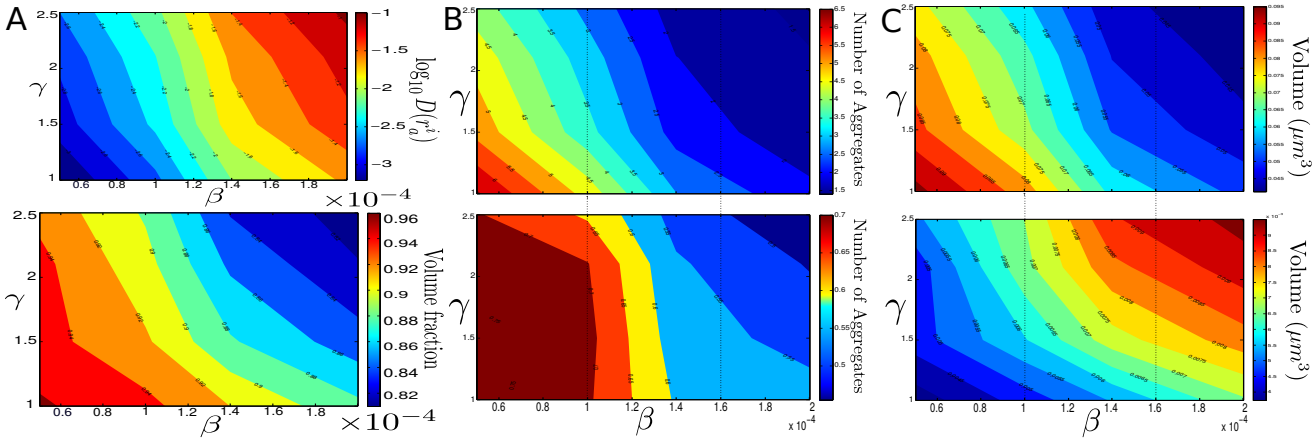

Figure S3: Dependence on the diffusion coefficient. A. Logarithm of the diffusion rate of an aggregate with radius r_a^i (top) and fraction of volume inside the mother cells (bottom) at the end of the cell division cycle. B-C. Number of aggregates and total aggregate volume inside mother cell (top) and inside the daughter cell (bottom) at the end of the cell division for different values of β and γ. $N = 1$, $\delta t = 0.5$, $\tau_m = 12$ min., $\tau_d = 120$ min. All other parameters were set to the values in Table S1. Results averaged over 1024 realizations.

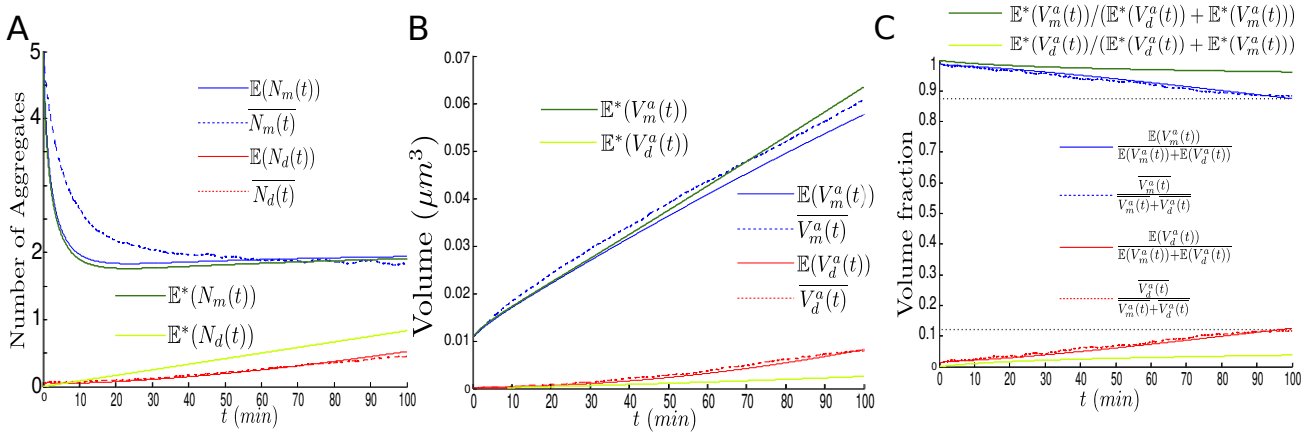

Figure S4: Aggregate kinetics under no cross-compartment transport. A-C. Same as in Fig. 3A-3C complemented with the results from numerically integrating Eq. S3 when assuming no cross-compartment transport. $N = 5$, $\tau_m = 12$ min., $\tau_d = 120$ min. All other parameters were set to the values in Table S1.

S7 Mathematical Analysis of confined diffusion in 2D

The MSD of a particle undergoing diffusion with rate D in d dimensional space follows $\left\langle r^2(t)\right\rangle_u = 2dDt$. Anomalous Diffusion corresponds to the case where $\left\langle r^2(t)\right\rangle = 2dDt^\alpha$, with $\alpha < 1$ (sub-diffusion) of $\alpha > 1$ (super-diffusion).
In 2D space, the MSD particle undergoing diffusion inside a disk of radius a can be found to be (9–11):

$$\left\langle r^2(t)\right\rangle_d = a^2\left(1 - 8\sum_{n\in\mathbb{Z}} \exp\left(\frac{-\beta_n^2 Dt}{a^2}\right)\frac{1}{\beta_n^2 - 1}\frac{J_0^2(\beta_n)}{J_1^2(\beta_n)}\right).$$

Where $J_i(x)$ denotes the i-th Bessel function of the first kind and the β_n's are the zeros of $J_1'(x)$.
In the case of diffusion inside an annulus with outer and inner radii a and b respectively, following the work done in (11–13), we are able to approximate $\left\langle r^2(t)\right\rangle$ at intermediate or large timescales as $\left\langle r^2(t)\right\rangle \simeq C(1 - \exp(-2\omega Dt))$, where C and ω are positive constants. As proven in (11), $C = \lim_{t\to\infty}\left\langle r^2(t)\right\rangle = 2R_G^2$, where R_G is the radius of gyration of the domain (the annulus) whereas ω is related to the degree of sub-diffusion at intermediate stages (which can be computed using curve fitting tools given its difficulty).

S8 Growth proportional to surface area

We believe that a constant rate of growth in volume is more consistent with the period of relaxation after heat or oxidative stress since, relative to the aggregate's size, initially growth happens fast (for many aggregates) and then slow for fewer larger aggregates after fusion events. In contrast, growth proportional to the surface area could be more consistent with aggregate growth at lower rates in WT unperturbed cells. For this purpose we introduce the following model.

We modify the rate of volume growth so that it is proportional to the surface area of the aggregate. Since the surface area of a sphere of radius r is $A = 4\pi r^2$, we now let the volume of an aggregate increase according to $dV/dt = (r(t)^2/(r_a^i)^2)C_c$. Here, in order for $r(\tau_c) = r_a^i$, $C_c = C_c = \frac{4\pi(r_a^i)^3}{\tau_c}$ (so a factor of 3 larger than in the original version of the model). The mathematical approximation for the dynamics of this variant takes the following form:

$$\begin{cases} \frac{dN_m(t)}{dt} = \frac{1}{\tau_m} - p_b N_m(t) \max(N_m(t) - 1, 0) \frac{16\pi r_m(t) D(r_m(t))}{V_1} - \kappa_m(t) N_m(t) + \kappa_d(t) N_d(t) \\ \frac{dN_d(t)}{dt} = \frac{1}{\tau_d} - p_b N_d(t) \max(N_d(t) - 1, 0) \frac{16\pi r_d(t) D(r_d(t))}{V_2(t)} - \kappa_d(t) N_d(t) + \kappa_m(t) N_m(t) \\ \frac{dV_m^a(t)}{dt} = C_m(r_m(t)^2/(r_a^i)^2) N_m(t) - \kappa_m(t) N_m(t) \langle V(t) \rangle_m + \kappa_d(t) N_d(t) \langle V(t) \rangle_d + \frac{1}{\tau_m} V_a^i \\ \frac{dV_d^a(t)}{dt} = C_d(r_d(t)^2/(r_a^i)^2) N_d(t) - \kappa_d(t) N_d(t) \langle V(t) \rangle_d + \kappa_m(t) N_m(t) \langle V(t) \rangle_m + \frac{1}{\tau_d} V_a^i \end{cases} \tag{S3}$$

As observed in Fig. S5, the consistency between the numerical and mathematical approximations remains remarkable. Besides aggregate volume growth, which is now growing exponentially (and hence the fraction of volume in the mother increases as well), all other results and conclusions remain unvaried. Fusion remains frequent, and the MSD slows down at intermediate and long timescales. In this case, the MSD reaches a higher value and rises faster since we only consider one initial aggregate instead of five. Thus, the aggregate experiences faster diffusion at small timescales and a stronger deceleration given the increasing volume growth rate.

Concerning Fig. S6, all results are equivalent to those in the original model –when decreasing slightly the growth rates, given that exponential growth occurs at longer timescales–, except for the number of crossings. Since, for smaller values of τ_m aggregates grow very fast, the number of crossings is significantly reduced as a function of τ_m. Nevertheless, the number of crossings remains orders of magnitude higher than the experimental observations in (14).

With respect to the the dependence on other parameters (e_l, δt and β and γ), almost all the observations above remain, with the exception of the aggregate volume growth, which is now higher for higher diffusion values (Fig. S7B). Accumulation in the mother is favored with increased size and fusion and the appearance of larger aggregates.

Finally, as observed in Fig. S8 and Fig. S9, all observations made in the original model regarding active-quality-control remain valid when aggregate growth is proportional to the surface area (and under smaller rates of growth). Indeed, the MSD remains consistent with sub-diffusion in all three cases, one aggregate deposit forms and is maintained in the mother cell, the number of crossings is significantly reduced to values matching experimental data, and the probability of inheritance by the bud of the largest aggregate drops to values near 0.02.

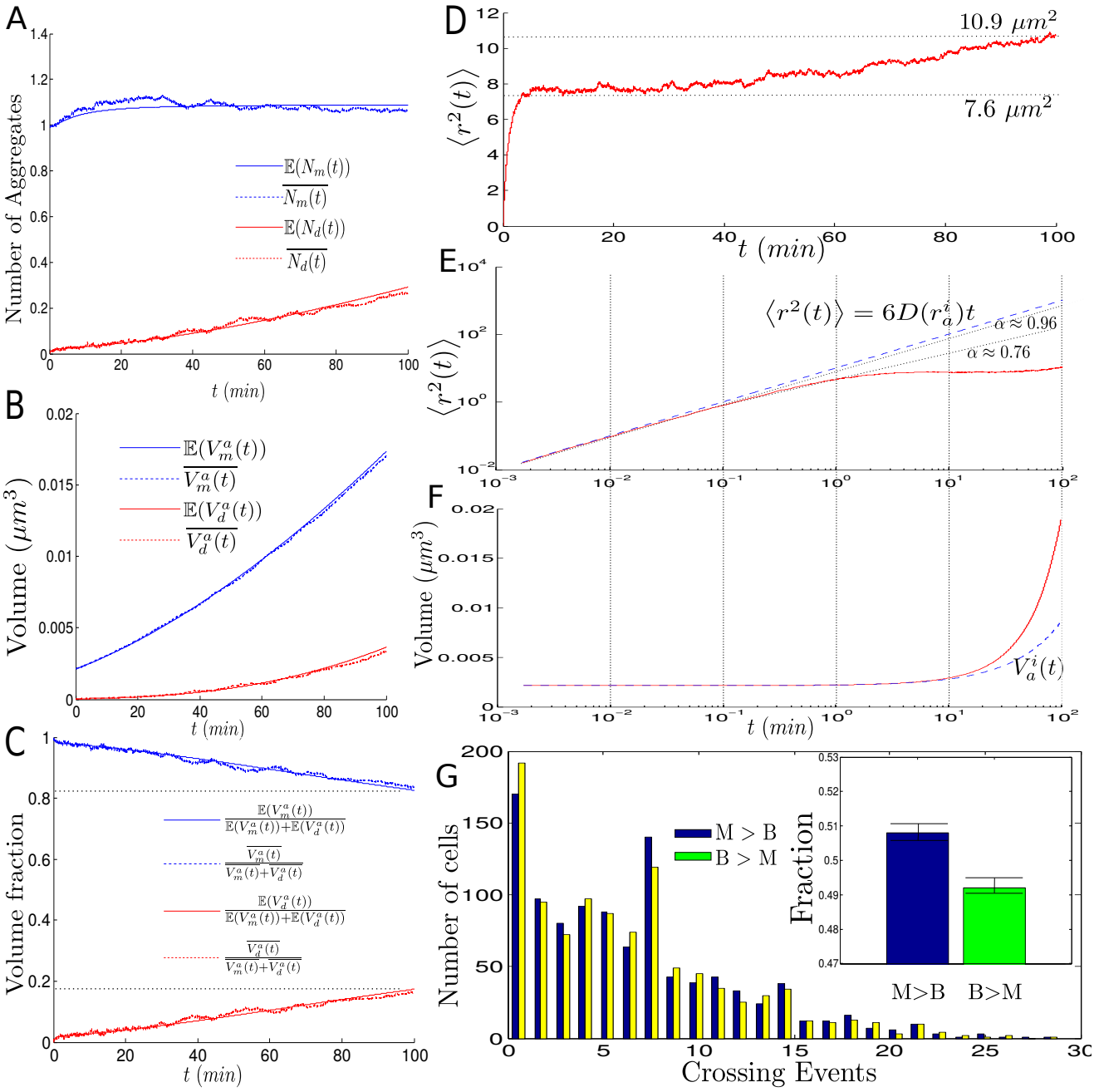

Figure S5: Single-division aggregate dynamics of the model with aggregate growth proportional to surface area. A-C. Number of aggregates, total aggregate volume and fraction of the total aggregate volume inside the mother (blue) and the daughter cell (red). Continuous line corresponds to the analytical prediction from the mathematical model with growth proportional to the surface area when numerically integrating Eq. S3. Dotted line corresponds to the numerical average from the simulations of the short-term aggregate dynamics. D. MSD of one aggregate throughout the short-term aggregate dynamics of the model corresponding to a single cycle of cell division. E-F. Log-log plot of Fig. S5D (top) and volume of the same aggregate for which the MSD was computed (bottom). Dashed lines correspond to the MSD of an aggregate of radius r_a^i (top) and to the volume of one aggregate with initial radius r_a^i in absence of fusion events. G. Histogram of total number of cross-compartment events from mother to bud ($M > B$) and from bud to mother ($B > M$). H Inset. Fraction of total cross-compartment events in each direction. In all figures, $N = 1$, $\delta t = 0.1$ sec., $\tau_m = 100$ min., $\tau_d = 1000$ min. All other parameters were set to the values in Table S1. Results averaged over 1024 realizations.

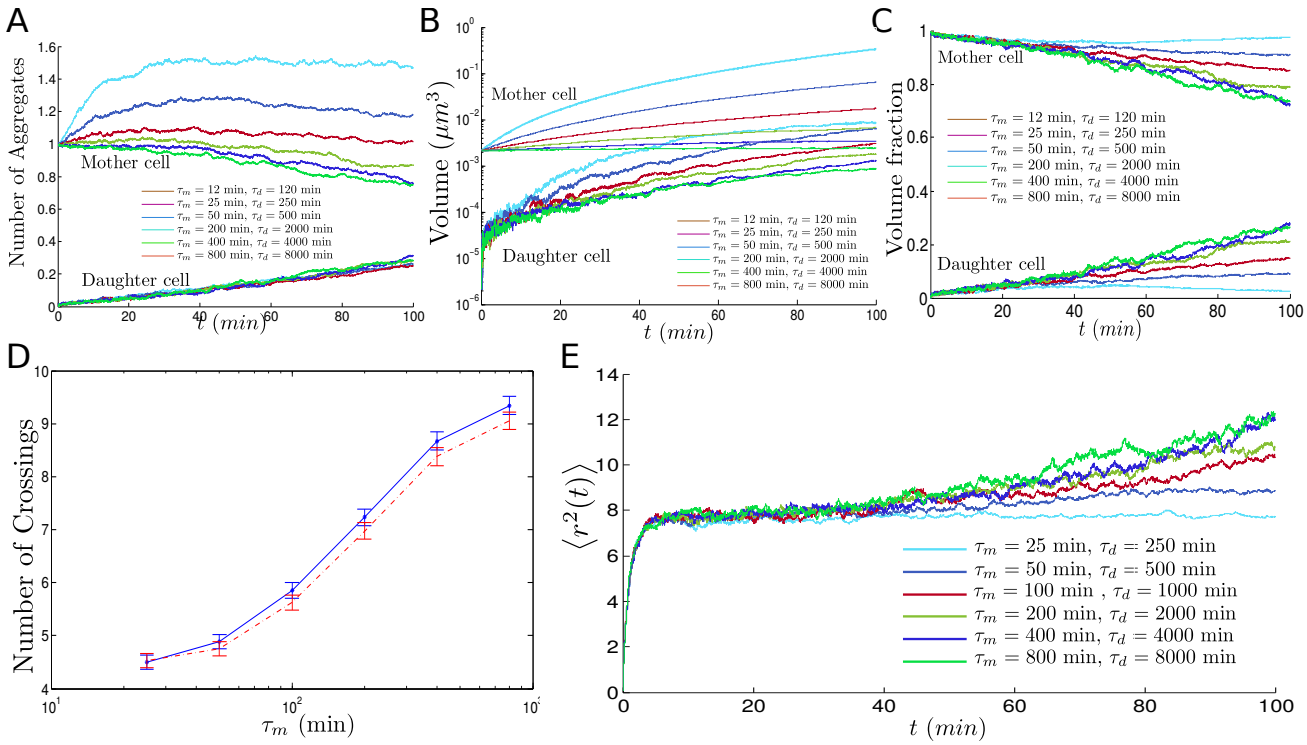

Figure S6: Single-division aggregate dynamics; dependence on the rate of appearance and growth of aggregates when growth is proportional to surface area. A-C. Number of aggregates, total aggregate volume and fraction of the total aggregate volume inside the mother and the daughter cell. D. Number of crossing events from mother to daughter (blue line) and from daughter to mother (red dashed line). E. MSD of one aggregate throughout the short-term component of the model corresponding to a single cycle of cell division for different rates of appearance and growth of aggregates. In all figures $N = 1$, $\delta t = 0.25$ sec. All other parameters were set to the values in Table S1. Results averaged over 1024 realizations.

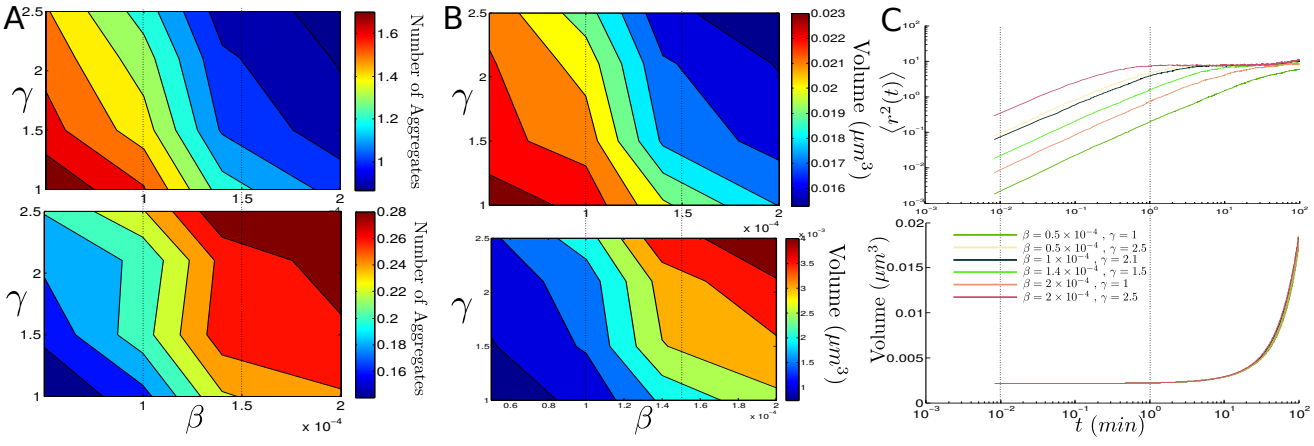

Figure S7: Dependence on diffusion coefficient continued when growth is proportional to surface area. A-B. Number of aggregates and total aggregate volume inside mother cell (top) and inside the daughter cell (bottom) at the end of the cell division for different values of β and γ. C. MSD of one aggregate throughout the short-term component of the model corresponding to a single cycle of cell division (top) and volume of the same aggregate for which the MSD was computed (bottom) for different values of β and γ. $N = 1$, $\delta t = 0.5$, $\tau_m = 100$ min., $\tau_d = 1000$ min. All other parameters were set to the values in Table S1. Results averaged over 1024 realizations.

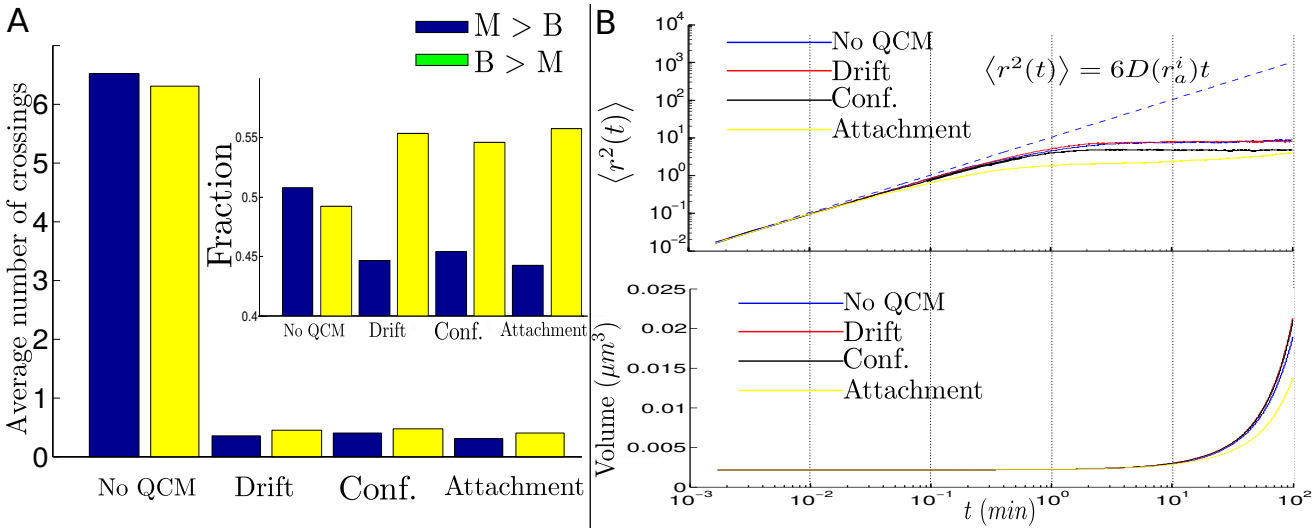

Figure S8: Single-division aggregate dynamics; Quality-control-mechanisms with aggregate growth proportional to surface area. A. Average number of crossing events from mother to bud ($M > B$) and from bud to mother ($B > M$) under different quality control mechanisms. Inset. Proportion of crossing events in both directions under different quality control mechanisms. B. MSD of one aggregate throughout a single cycle of cell division and volume of the same aggregate for which the MSD was computed for different quality-control-mechanisms. Dashed line corresponds to the MSD of an aggregate of radius r_a^i (top). In all simulations, $N = 1$, $\delta t = 0.1$ sec., $\tau_m = 100$ min., $\tau_d = 1000$ min. All other parameters were set to the values in Table S1. Results averaged over 1024 realizations.

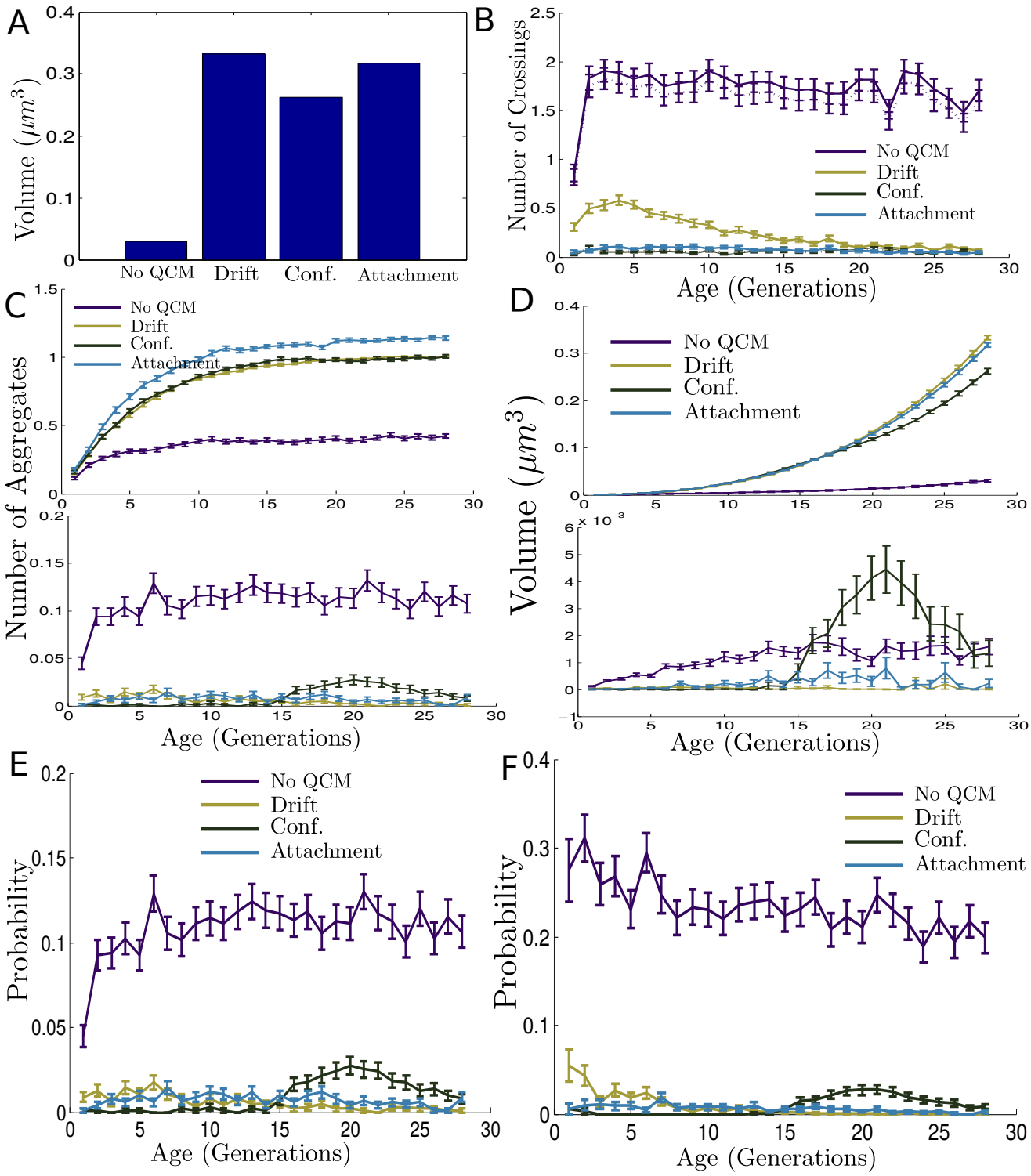

Figure S9: Variants of the model with active-quality-control mechanisms and aggregate growth proportional to surface area. A. Total aggregate volume inside the mother cell at the end of the 28th division for different QCMs. B. Number of crossing events from mother to bud (continuous line) and from bud to mother (dotted line) as a function of the mother's age (in generations) for different QCMs. C-D. Total number of aggregates and total aggregate volume inside the mother cell (top) and inside the daughter cell (bottom) as a function of the mother's age (in generations) for different QCMs. E. Probability of inheritance of at least one aggregate by the daughter cell at the end of cell division as a function of the mother's age (in generations) for different QCMs. F. Probability of inheritance of the largest aggregate by the daughter cell, when in presence of aggregates, as a function of the mother's age (in generations) for different QCMs. Error bars correspond to the Standard error. In all simulations $\delta t = 0.5$, $\tau_m = 800$ min., $\tau_d = 8000$ min., all other parameters were set to the values in Table S1. Results averaged over 1024 realizations.

Supporting References

1. Paoletti, C., S. Quintin, A. Matifas, and G. Charvin, 2016. Kinetics of formation and asymmetrical distribution of hsp104-bound protein aggregates in yeast. *Biophysical journal*, 110(7):1605–1614.

2. Coelho, M., S. J. Lade, S. Alberti, T. Gross, and I. M. Tolić, 2014. Fusion of protein aggregates facilitates asymmetric damage segregation. *PLoS Biol*, 12(6):e1001886.

3. Schuss, Z., A. Singer, and D. Holcman, 2007. The narrow escape problem for diffusion in cellular microdomains. *Proceedings of the National Academy of Sciences*, 104(41):16098–16103.

4. Schuss, Z., 2010. Equilibrium and recrossings of the transition state: What can be learned from diffusion?. *The Journal of Physical Chemistry C*, 114(48):20320–20334.

5. Lovrics, A., A. Csikász-Nagy, I. G. Zsély, J. Zádor, T. Turányi, and B. Novák, 2006. Time scale and dimension analysis of a budding yeast cell cycle model. *BMC bioinformatics*, 7(1):494.

6. Saarikangas, J., F. Caudron, R. Prasad, D. F. Moreno, A. Bolognesi, M. Aldea, and Y. Barral, 2017. Compartmentalization of er-bound chaperone confines protein deposit formation to the aging yeast cell. *Current Biology*, 27(6):773–783.

7. Saarikangas, J. and Y. Barral, 2015. Protein aggregates are associated with replicative aging without compromising protein quality control. *Elife*, 4:e06197.

8. Erjavec, N., L. Larsson, J. Grantham, and T. Nyström, 2007. Accelerated aging and failure to segregate damaged proteins in sir2 mutants can be suppressed by overproducing the protein aggregation-remodeling factor hsp104p. *Genes & development*, 21(19):2410–2421.

9. Bickel, T., 2007. A note on confined diffusion. *Physica A: Statistical Mechanics and its Applications*, 377(1):24–32.

10. Riseborough, P. S. and P. Hanggi, 1982. Diffusion on surfaces of finite size: Mössbauer effect as a probe. *Surface Science*, 122(3):459–473.

11. Saxton, M. J., 1993. Lateral diffusion in an archipelago. single-particle diffusion. *Biophysical journal*, 64(6):1766–1780.

12. Spokoini, R., O. Moldavski, Y. Nahmias, J. L. England, M. Schuldiner, and D. Kaganovich, 2012. Confinement to organelle-associated inclusion structures mediates asymmetric inheritance of aggregated protein in budding yeast. *Cell reports*, 2(4):738–747.

13. Kusumi, A., Y. Sako, and M. Yamamoto, 1993. Confined lateral diffusion of membrane receptors as studied by single particle tracking (nanovid microscopy). effects of calcium-induced differentiation in cultured epithelial cells. *Biophysical journal*, 65(5):2021.

14. Zhou, C., B. D. Slaughter, J. R. Unruh, A. Eldakak, B. Rubinstein, and R. Li, 2011. Motility and segregation of hsp104-associated protein aggregates in budding yeast. *Cell*, 147(5):1186–1196.

15. Kinkhabwala, A., A. Khmelinskii, and M. Knop, 2014. Analytical model for macromolecular partitioning during yeast cell division. *BMC biophysics*, 7(1):10.

16. Liu, B., L. Larsson, A. Caballero, X. Hao, D. Öling, J. Grantham, and T. Nyström, 2010. The polarisome is required for segregation and retrograde transport of protein aggregates. *Cell*, 140(2):257–267.